The Journal of Chemical Physics

Li-diffusion at the interface between Li-metal and [Pyr_{14}][TFSI]-ionic liquid: *Ab initio* molecular dynamics simulations

Cite as: J. Chem. Phys. **152**, 031101 (2020); https://doi.org/10.1063/1.5132566
Submitted: 18 October 2019 . Accepted: 27 December 2019 . Published Online: 16 January 2020

Boris V. Merinov, Saber Naserifar, Sergey V. Zybin, Sergey Morozov, William A. Goddard, Jinuk Lee, Jae Hyun Lee, Hyea Eun Han, Young Cheol Choi, and Seung Ha Kim

View Online Export Citation CrossMark

© 2020 Author(s).

AIP Publishing

The Journal of Chemical Physics COMMUNICATION scitation.org/journal/jcp

Li-diffusion at the interface between Li-metal and [Pyr_{14}][TFSI]-ionic liquid: *Ab initio* molecular dynamics simulations

Cite as: J. Chem. Phys. 152, 031101 (2020); doi: 10.1063/1.5132566
Submitted: 18 October 2019 • Accepted: 27 December 2019 •
Published Online: 16 January 2020

View Online Export Citation CrossMark

Boris V. Merinov,[1,a] Saber Naserifar,[1] Sergey V. Zybin,[1] Sergey Morozov,[2] William A. Goddard III,[1] Jinuk Lee,[3] Jae Hyun Lee,[3] Hyea Eun Han,[3] Young Cheol Choi,[3] and Seung Ha Kim[3]

AFFILIATIONS

[1]Materials and Process Simulation Center (MSC), California Institute of Technology (Caltech), Pasadena, California 91125, USA
[2]South Ural State University, 76 Lenin Avenue, Chelyabinsk 454080, Russia
[3]Battery R&D, LG Chem, Yuseong-Gu, Daejeon 34122, South Korea

[a]E-mail: merinov@caltech.edu

ABSTRACT

We previously reported comprehensive density functional theory-molecular dynamics (DFT-MD) at 400 K to determine the composition and structure of the solid electrolyte interface (SEI) between a Li anode and [Pyr_{14}][TFSI] ionic liquid. In this paper, we examined diffusion rates in both the Li-electrode region and SEI compact layer in smaller 83Li/2[TFSI] and larger 164Li/4[TFSI] systems. At 400 K, the Li-diffusion constant in the Li-region is 1.35×10^{-10} m^2/s for 83Li/2[TFSI] and 5.64×10^{-10} m^2/s for 164Li/4[TFSI], while for the SEI it is 0.33×10^{-10} m^2/s and 0.22×10^{-10} m^2/s, thus about one order slower in the SEI compared to the Li-region. This Li-diffusion is dominated by hopping from the neighbor shell of one F or O to the neighbor shell of another. Comparing the Li-diffusion at different temperatures, we find that the activation energy is 0.03 and 0.11 eV for the Li-region in the smaller and larger systems, respectively, while for the SEI it is 0.09 and 0.06 eV.

Published under license by AIP Publishing. https://doi.org/10.1063/1.5132566

Application of ionic liquids (ILs) as electrolyte in Li-batteries provides a number of advantages compared to liquid electrolytes used in the current battery technology.[1–4] One of the most important battery components is the solid electrolyte interface (SEI), which is formed on lithium and graphite anodes as a result of decomposition of electrolyte materials.[5,6] The SEI plays an important role, preventing the Li-based electrode from comprehensive oxidation and the electrolyte from further extensive decomposition. Numerous studies show that the electrode/electrolyte interface remains the most critical part of electrochemical devices (see, for instance, Refs. 7–11). However, processes of SEI formation and growth are still not fully understood, especially the SEI structure and morphology evolution and Li-ion diffusion inside the SEI layer. It is generally accepted to consider the SEI as consisting of two layers, compact (inorganic solid phase) and porous (organic-containing phase).[7,8,12–14] The compact layer forms close to the electrode surface and is assumed to be ~10 Å thick.[12] The porous layer grows on top of the compact layer and has a higher Li-ion diffusion coefficient than that of the compact layer, but lower electronic conductivity.[7] Only limited information is available about the SEI composition and structure. Similarly, investigations focusing on Li-ion migration and diffusion behavior across the interface are insufficient to draw firm conclusions about the mechanisms and pathways for the Li-ion transport through the SEI, including systems with ILs. Therefore, atomic-level understanding of the interface structure and ion diffusion is essential for further design of the optimal SEI leading to the best battery performance. In our previous study,[15] we determined the atomistic structure of the Li-metal/[Pyr_{14}][TFSI]-IL interface, in particular, the SEI compact (inner) layer (SEI CL), using density functional theory based molecular dynamics (DFT-MD, also called *ab initio* MD) simulations. Initially, the bcc Li-metal and lithium bis(trifluoromethanesulfonyl)imide (LiTFSI) salt were used to build

Published under license by AIP Publishing

the Li/IL interface. During the SEI CL formation, the surface Li atoms reacted with TFSI anions and migrated to the SEI CL. The vacancies formed after this migration moved to the bulk Li. As a result, the Li-metal region became highly disordered and capture features of the amorphouslike (or quasiamorphous) structure rather than the regular crystalline, which requires the long-range order. It is similar to the formation of the Li-SEI interface observed by Shi *et al.* in both carbonate and ether-based electrolytes[16] and consistent with the point defect model for metal dissolution with a passivation layer developed by Macdonald.[17]

The SEI CL structure, found in our simulations, is highly disordered and mostly consists of LiF and Li_2O aggregates (blocks) with addition of the S, N, and C anions bonded with Li. These blocks are composed of the same structural units as in the corresponding crystalline phases and have the short-range order, but the whole SEI CL structure, as is mentioned above, is highly disordered and does not have the long-range order, which makes it amorphouslike (or quasiamorphous). Our findings are consistent with the above-mentioned model developed by Macdonald[17] and the experimental results obtained by Howlett *et al.*[18] for the SEI formed on a Li electrode in the IL. They found that the inner layers formed rapidly under less selective conditions and were composed of species with less complex chemical structures, such as Li_2O, LiF, etc. These conditions produce a layer that has the greatest amount of defects present in its structure due to the less selective formation conditions.

In this letter, we report our DFT-MD results on the Li-ion diffusion rates at the interface between a Li electrode and $[Pyr_{14}][TFSI]$ IL. Similar to Ref. 15, two systems will be considered:

- a smaller system with 83 Li and 2 [TFSI] for which it was practical to run a much longer DFT-MD simulation, 723 ps, and
- a larger system with 164 Li and 4 [TFSI], where we reported a DFT-MD simulation for 164 ps. This system enabled better distinction between the Li-metal and SEI regions and between the corresponding Li-ion self-diffusion coefficients.

Figure 1 shows self-diffusion coefficients of all elements (C, F, O, N, S, and Li) calculated from the corresponding mean square displacements (MSD) in the smaller and larger Li/IL systems (see also Table S1 in the supplementary material). The diffusion coefficients for the smaller and larger systems show comparable tendencies and both illustrate a significantly higher diffusion of lithium compared to the other ions. First, we will analyze the Li-ion self-diffusion in the smaller 83Li/2[TFSI] system and then in the larger 164Li/4[TFSI] system.

DFT-MD on the smaller 83Li/2[TFSI] system. The SEI CL architecture, obtained in our simulations, is dominantly built by Li, F, and O atoms (Fig. 2). The chemical composition of the SEI CL is similar to that observed in conventional Li-ion batteries with the liquid electrolyte and graphite-based electrode,[19–29] except for a limited number of S, N, and C atoms presented in the SEI CL of the Li/IL interface. It was reported that $(CH_2CH_2OCO_2Li)_2$, $(CH_2OCO_2Li)_2$, $LiO(CH_2)_2CO_2(CH_2)_2OCO_2Li$, $Li(CH_2)_2OCO_2Li$, CH_3OLi, LiOH, $(CH_2OCOOCH_3)_2$, and $(CH_2CH_2O)_2$ initially formed on the graphite surface were replaced by Li_2CO_3, Li_2O, and LiF. Li_2CO_3 could easily be decomposed into Li_2O.[7,19] Thus, the constituents of the surface films nearest to the graphite surface will eventually be completely transformed to Li_2O and LiF,[19] which has been experimentally confirmed by XPS measurements.[30,31]

The Li-ion self-diffusion in the smaller 83Li/2[TFSI] system was determined from the 723 ps NVT DFT-MD at 400 K (Fig. 3). Because the Li-metal region is relatively narrow in this system, some of the Li atoms are in the SEI for part of time and in the Li-metal region for another part of time. This leads to certain uncertainty and as a result, distinction between the Li atoms belonging either to the SEI CL or to the Li-metal region is contingent for some Li atoms. Nonetheless, we separated these two regions (see the inset in Fig. 3), keeping in mind this uncertainty, and found that the Li-diffusion in the SEI CL (D_{SEI}) was 4 times slower than in the Li-metal region ($D_{Li\text{-}metal}$), 0.33×10^{-10} vs 1.35×10^{-10} m^2/s (Table I and Figs. S1 and S2 in the supplementary material).

Analyzing the trajectory, we concluded that the most significant contribution to the D_{SEI} came from the vacancy-mediated diffusion mechanism. This conclusion is similar to that made by Benitez and Seminarioa for Li_2CO_3, LiF, and Li_2O.[20] The F and O anions in the SEI are typically coordinated with 3 or 4 Li atoms and with 4–6 Li atoms, respectively.[15] Therefore, for example, a Li_4O group has ability to accept up to two additional Li atoms. During thermal vibrations (atomic motion) of this group, the corresponding Li atoms may shift in such a way that enough space is formed between the Li atoms and there appears an opportunity for a Li atom from another Li_nX group (X = F, O, N, S, and C) to jump to this vacant place, forming in turn a new vacancy in the Li_nX group, which will be later occupied by another Li atom.

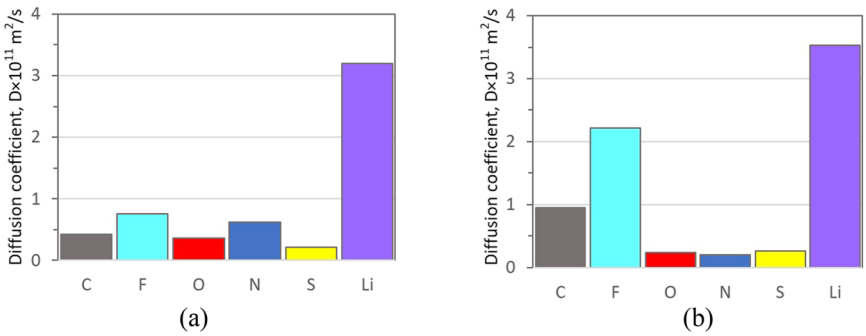

FIG. 1. Ion self-diffusion coefficients in the (a) smaller 83Li/2[TFSI] and (b) larger 164Li/4[TFSI] systems at 400 K.

Published under license by AIP Publishing

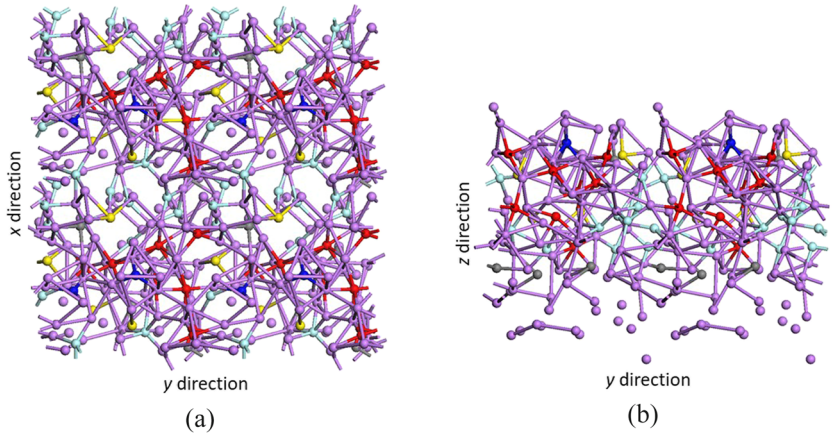

FIG. 2. SEI compact layer structure (2 × 2 × 1) (a) view along the *z*-direction and (b) view along the *x*-direction.

To estimate the Li diffusion activation energy (E_a), we performed a DFT-MD simulation on the 83Li/2[TFSI] system for 554 ps at 300 K in addition to 400 K. The calculated D_{SEI} value at 300 K is 0.14×10^{-10} m^2/s, while for the Li-metal region $D_{Li\text{-}metal}$ is 0.97×10^{-10} m^2/s. We realize that the two temperature points provide only a rough value for this parameter. On the other hand, we believe that adding one more temperature point between 300 K and 400 K will not change significantly the value of the activation energy. AIMD simulations are very time-consuming and running long simulations at additional temperature points similar to those at 400 and 300 K to estimate E_a would be impractical. Instead, we applied another method, 2PT, which gave comparable diffusivity and activation energy values using much shorter time intervals (see Table I and the related section below).

To enhance credibility of our results, we performed a shorter DFT-MD simulation (355 ps) on the smaller system at 350 K and calculated the corresponding Li diffusivity. As we expected, adding the third temperature point changed the activation energy only negligibly. The obtained values are as follows: $D_{SEI} = 0.30 \times 10^{-10}$ m^2/s and $D_{Li\text{-}metal} = 1.02 \times 10^{-10}$ m^2/s at 350 K, and $E_a = 0.09$ and 0.03 eV, for the SEI CL and Li-metal region, respectively (see Figs. S3 and S4 in the supplementary material).

DFT-MD on the larger 164Li/4[TFSI] system. The larger Li/IL system enables us to better separate the Li-metal and SEI regions of the system (Fig. 4) and analyze the related Li-diffusions. We find that the D_{SEI} values for the larger 164Li/4[TFSI] system, 0.12×10^{-10} m^2/s at 300 K and 0.22×10^{-10} m^2/s at 400 K, are close to the values for the smaller 83Li/2[TFSI] system, 0.14×10^{-10} m^2/s at 300 K and 0.33×10^{-10} m^2/s at 400 K and over one order of magnitude lower than the $D_{Li\text{-}metal}$ values, 1.95×10^{-10} at 300 K and 5.64×10^{-10} m^2/s at 400 K. E_a, calculated from these data, is 0.06 eV for the SEI CL and 0.11 eV for the Li-metal region (Table I and Figs. S5 and S6 in the supplementary material). Note again that due to a large number of vacancies, the Li-metal region is

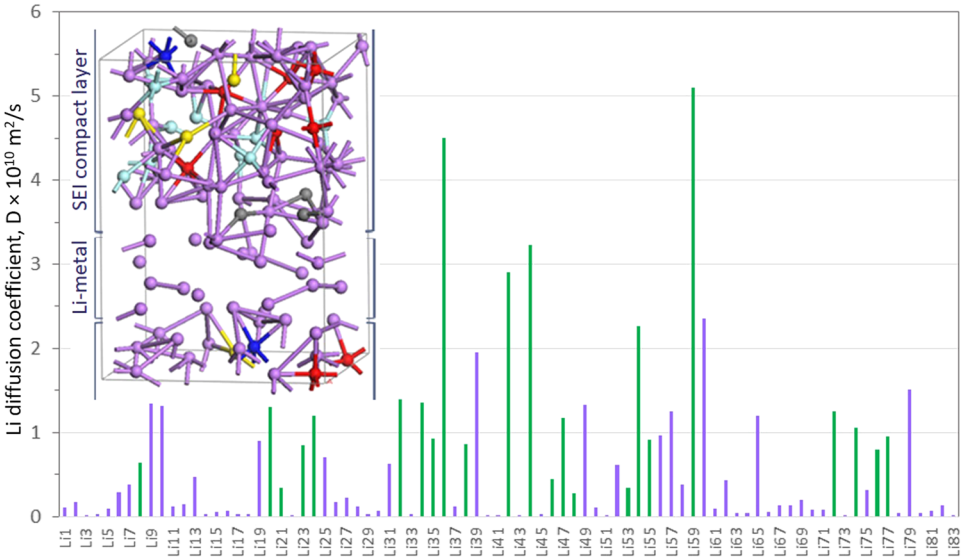

FIG. 3. Li-diffusion coefficients for each Li atom of the smaller 83Li/2[TFSI] system. Green: Li atoms in the Li-metal region and purple: Li atoms in the SEI compact layer. The inset is the Li/IL interface structure after 723 ps DFT-MD at 400 K.

Published under license by AIP Publishing

TABLE I. Li diffusivity in the 164Li/4[TFSI] and 83Li/2[TFSI] systems computed for the Li-metal region ($D_{Li\text{-}metal}$) and SEI compact layer (D_{SEI}) at 300 and 400 K, and the corresponding activation energy (E_a). The estimated error in the diffusivity data is $\pm 0.1 \times 10^{-10}$ m^2/s for the SEI CL and $\pm 1.1 \times 10^{-10}$ m^2/s for the Li-metal region.

	Interval (ps)				E_a (eV)	
System	MSD	2PT	$D_{Li\text{-}metal} \times 10^{10}$ (m^2/s)	$D_{SEI} \times 10^{10}$ (m^2/s)	Li-metal	SEI
			400 K			
164Li/4[TFSI]	42–164		5.64	0.22	0.11	0.06
		144–164	5.14	0.34	0.09	0
83Li/2[TFSI]	393–723		1.35	0.33	0.03	0.09
		443–463	3.08	0.38	0.03	0.03
			300 K			
164Li/4[TFSI]	10–73		1.95	0.12		
		45–65	3.14	0.34		
83Li/2[TFSI]	222–554		0.97	0.14		
		272–292	2.39	0.30		

highly disordered in our simulation and should be considered as quasiamorphous, not as regular crystalline.

The Li-ion diffusion mechanism in the SEI CL of the larger 164Li/4[TFSI] system looks similar to that described above for the smaller 83Li/2[TFSI] system.

Computation of Li-ion diffusivity from density of states. In addition to the conventional MSD method, we used the density of states (DoS) of atoms to compute the Li diffusion coefficients. The two-phases thermodynamics (2PT) methodology[32–36] (see the computational method section) was applied to calculate the power spectrum as a function of frequency, DoS(υ). From the 2PT analysis, we also determined the Li diffusivity for both larger 164Li/4[TFSI] and smaller 83Li/2[TFSI] systems at 300 and 400 K, employing the DoS(υ) at zero frequency, DoS(0) = $12mND/kT$. For each of these systems, we computed $D_{Li\text{-}metal}$ and D_{SEI}, using a 20 ps interval of the related DFT-MD trajectories. The results are summarized in Table I.

For the smaller 83Li/2[TFSI] system, we obtained $D_{Li\text{-}metal} = 3.08 \times 10^{-10}$ m^2/s and $D_{SEI} = 0.38 \times 10^{-10}$ m^2/s at 400 K, and $D_{Li\text{-}metal} = 2.39 \times 10^{-10}$ and $D_{SEI} = 0.30 \times 10^{-10}$ m^2/s at 300 K, using the 2PT method. These values are comparable with those obtained from the MSD, where $D_{Li\text{-}metal} = 1.35 \times 10^{-10}$ m^2/s and

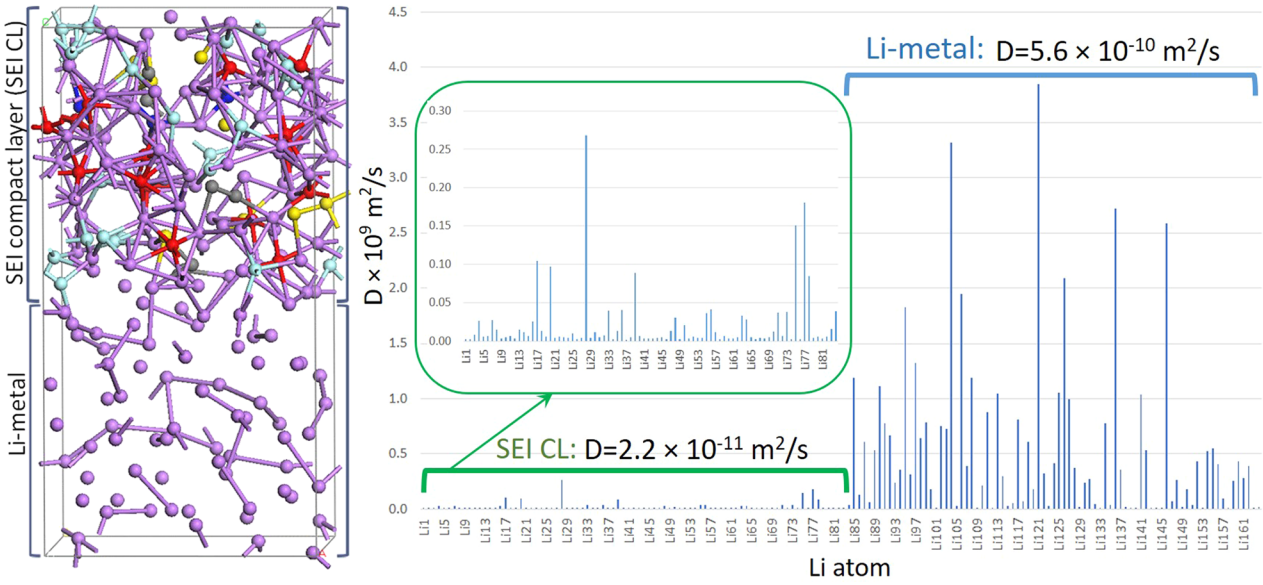

FIG. 4. Diffusion coefficient (D) for each Li atom in the larger 164Li/4[TFSI] system at 400 K.

Published under license by AIP Publishing

$D_{SEI} = 0.33 \times 10^{-10}$ m^2/s at 400 K, and $D_{Li\text{-}metal} = 0.97 \times 10^{-10}$ m^2/s and $D_{SEI} = 0.14 \times 10^{-10}$ m^2/s at 300 K. As expected, both $D_{Li\text{-}metal}$ and D_{SEI} are higher (1.3 times) at 400 K compared to 300 K. The calculated E_a for the Li-diffusion in the Li-metal region is 0.03 eV based on the both 2PT and MSD, while for the SEI CL, E_a is 0.03 and 0.09 eV for the 2PT and MSD, respectively (Table I and Figs. S3, S4, S7, and S8 in the supplementary material).

The larger 164Li/4[TFSI] system obviously enables us to better separate the Li-metal region and SEI CL and $D_{Li\text{-}metal}$ and D_{SEI} computed from MSD are 5.64×10^{-10} and 0.22×10^{-10} m^2/s at 400 K, and 1.95×10^{-10} and 0.12×10^{-10} m^2/s at 300 K. The associated E_a is 0.11 and 0.06 eV for the Li-metal region and SEI CL, respectively. The corresponding values from 2PT are 5.14×10^{-10} and 0.34×10^{-10} m^2/s at 400 K, and 3.14×10^{-10} and 0.34×10^{-10} m^2/s at 300 K, and E_a is 0.09 and 0.00 eV (because D_{SEI} has the same value, 0.34×10^{-10} m^2/s, from 2PT at 400 and 300 K) for the Li-metal region and SEI CL, respectively (Table I and Figs. S4, S5, S9, and S10 in the supplementary material). Similar to the smaller 83Li/2[TFSI] system, $D_{Li\text{-}metal}$ in the larger 164Li/4[TFSI] system is 1.6 times higher at 400 K compared to 300 K.

For all cases and temperatures, $D_{Li\text{-}metal}$ is approximately one order of magnitude higher than D_{SEI}.

We also computed the diffusivity distribution of Li atoms to provide a better understanding of the atomic contributions to $D_{Li\text{-}metal}$ and D_{SEI} (Fig. 5). The results for 164Li/4[TFSI] at 300 and 400 K show very resembling behavior. The first peak for both $D_{Li\text{-}metal}$ and D_{SEI} looks similar with the maximum around 0.5×10^{-10} m^2/s and the first minimum around 1.2×10^{-10} m^2/s for both temperatures [Figs. 5(a) and 5(b)]. However, there are several Li atoms in the Li-metal region, which have much higher diffusivity (over 1.2×10^{-10} m^2/s) than that in the SEI CL. This results in the significantly higher values of $D_{Li\text{-}metal}$ compared to D_{SEI} (Table I).

For 83Li/2[TFSI] at 300 K, both Li-metal and SEI have the first peak around 0.3×10^{-10} m^2/s and the first minimum around 1.0×10^{-10} m^2/s. The Li atoms with diffusivities over 1.0×10^{-10} m^2/s are responsible for the overall larger value of $D_{Li\text{-}metal}$ compared to D_{SEI} (see Table I). At 400 K, the Li-metal first peak is at a slightly higher value of 0.5×10^{-10} m^2/s compared to that for the SEI CL, 0.3×10^{-10} m^2/s. Similar to 300 K, several Li atoms in the Li-metal region show diffusivities higher than 1.5×10^{-10} m^2/s, which leads to the significantly higher $D_{Li\text{-}metal}$ compared to D_{SEI}.

Comparison to other studies. As mentioned above, it was reported that the SEI CL consists of Li_2O and LiF in conventional Li-ion batteries.[19,30,31] Based on this conclusion, attempts to describe the Li transport in the SEI through the individual SEI compounds were undertaken using computational simulations of the Li-ion diffusion in crystalline Li_2O and LiF.[7,20] The reported

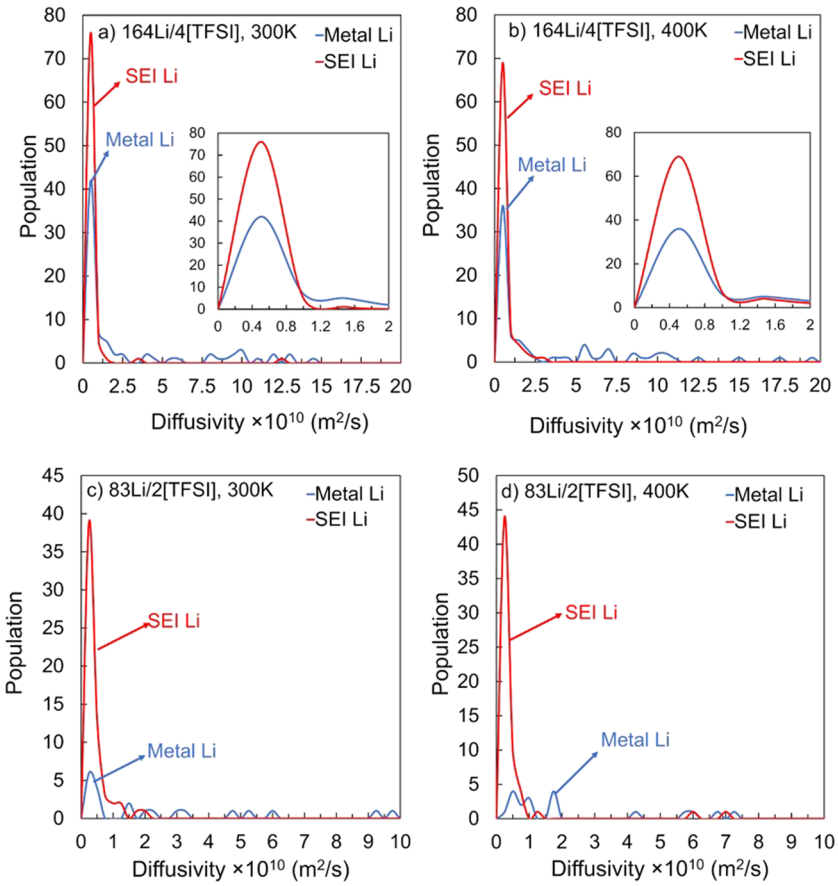

FIG. 5. Population distribution of Li atom diffusivities in the larger 164Li/4[TFSI] system at (a) 300 K for 45–65 ps and (b) 400 K for 144–164 ps, and in the smaller 83Li/2[TFSI] system at (c) 300 K for 50–70 ps and (d) 400 K for 50–70 ps. The difference in the height of the first peak corresponding to Li atoms in the Li-metal region (blue) and SEI compact layer (red) is due to a larger number of Li atoms in the SEI compact layer. The behavior of the first peak is similar in all cases.

Published under license by AIP Publishing

values of the Li-ion diffusion coefficient are ~10^{-12} m^2/s for Li_2O and three orders of magnitude lower for LiF.[20,37] LiF plays an important role in the morphological and compositional picture of the SEI and it may cause rate limitations in Li-ion batteries.[38,39] However, it should be noted that the SEI CL in the Li/IL systems is highly disordered and characterized by an amorphouslike structure with LiF and Li_2O fragments (aggregates), rather than by a regular crystal structure. Therefore, the related Li-diffusion should be faster than in the crystalline Li_2O and LiF compounds and we found it significantly faster in our simulations, 0.33×10^{-10} and 0.14×10^{-10} m^2/s at 400 and 300 K, respectively (Table I), because the corresponding Li, F, O-network is irregular and contains a number of vacancies (Fig. 2). The latter value is similar to that (0.1×10^{-10} m^2/s) for the Li diffusivity in $[Pyr_{14}][TFSI]$–[Li][TFSI] at 300 K measured via pulsed-field gradient-nuclear magnetic resonance (PFG-NMR).[40–42] Our results overlap with the results of the experimental study,[18] where it was found that the SEI layered structure, formed on a Li electrode in IL, became progressively more conductive (i.e., more disordered) close to the Li surface. The inner layer of the SEI is the most conductive because it has the greatest amount of defects so that the related activation energy for this region is expected to be low.[18] This conclusion is in excellent agreement with our computational results. Indeed, our DFT-MD simulations predict the highly disordered SEI CL structure to have relatively fast Li diffusion, ~10^{-11} m^2/s, with the corresponding E_a less than 0.1 eV (Table I). This E_a value is also comparable with 0.06 eV obtained from electrochemical impedance spectroscopy (EIS) for $[Pyr_{14}][TFSI]$–[Li][TFSI][43] and 0.04 eV calculated in Refs. 7 and 38 for the SEI solid phase in Li-ion batteries.

As for the Li-metal region, it is more relevant to compare the Li-ion diffusion parameters for the larger 164Li/4[TFS] system with the related published data, because the Li-metal region and SEI CL are better separated in this system. The Li-metal region is amorphous in our simulations and its diffusion coefficient, 1.95×10^{-10} m^2/s at 300 K, is in agreement with that in amorphous Li-based materials, such as $Li_{15}Si_4$, 3.0×10^{-10} m^2/s at 300 K,[44] where most of the Li is not bonded with Si and is expected to move relatively freely. Since the amorphous Li has a higher density of vacancies compared to the solid crystalline Li, it enables a Li atom occasionally to jump into a neighboring vacant site providing the relatively fast Li-diffusion in this phase. E_a of 0.11 eV agrees with that in amorphous Li, 0.2 eV for $Li_{15}Si_4$, which has a trend to decrease, when the Li fraction increases.[45]

Summarizing, the simulation results obtained for the Li-diffusion in the Li/IL systems using two different methods (MSD and 2PT) are consistent and in good agreement with the experimental result,[18,40–44] which increases confidence in credibility of our findings. This study is a part of the project in which we propose to use superionic sulfide ceramics, such as Li_6PS_5X (X = Cl, Br, I),[46–49] as a solid electrolyte and the ionic liquid as an interlayer to prevent the direct contact of the ceramics with a Li-metal anode. This would otherwise cause decomposition of the ceramics with concomitant degradation of the battery performance.[49–51] We believe that the use of the ionic liquid may provide a way to advance the current Li-ion battery technology toward a new generation of Li-metal batteries based on a solid electrolyte. The results, obtained in this and earlier published works (see, for instance, Refs. 11, 18, and 40–43) generally confirm that ionic liquids could efficiently be applied in a new generation of Li-metal batteries. Experimental methods, such as XPS, produce data only for the outer surface of a sample. Thus, much of the SEI structure, including the SEI compact (inner) layer, is not accessed. The available information on this interface is very limited and often ambiguous. Our AIMD computations provide descriptions of the both SEI layers separately, which is not yet possible experimentally. Therefore, the structure and diffusion properties of the SEI CL, obtained in our simulations, provide valuable information for optimizing the SEI in the Li/IL system that should lead to better battery performance.

Computational methods. To determine the transport property of the SEI at equilibrium density, we performed DFT-MD simulations using the Vienna *Ab Initio* Simulation Package (VASP),[52–54] which implements the projector augmented wave (PAW) method for DFT. For all DFT-MD simulations, we use the Perdew-Burke-Ernzerhof generalized gradient approximation (GGA-PBE)[54,55] with the D3 (Becke-Johnson) empirical corrections[56,57] for long-range pairwise van der Waals attractive forces (approximating the London dispersion). This PBE-D3 level of DFT has been validated for several molecular systems, including DFT-MD simulations of metal-organics and Li-ion battery interfaces in particular.[58–62]

The energy cutoff for the plane-wave basis expansion was chosen at 500 eV, which was verified to provide converged forces by a test calculation at 600 eV. For the bulk Brillouin zone integration, a Γ-centered 1 × 1 × 1 k-point mesh was used in all DFT-MD simulations within the supercell. A conjugate gradient algorithm was employed to relax the ion positions to obtain initial optimized structures. The initial velocities of the DFT-MD were chosen from the Maxwell–Boltzmann distribution with a temperature of 20 K. The temperature during DFT-MD was maintained using a Nose–Hoover thermostat. The procedures of obtaining the equilibrium 83Li/2[TFSI] and 164Li/4[TFSI] model systems were described in our previous work.[15] We performed DFT-MD simulations on these systems first at 400 K for 723 and 164 ps, respectively, and then at 300 K for 554 and 73 ps, respectively. In addition, the 355 ps DFT-MD simulation was performed on the smaller system at 350 K. Thus, the systems that we used in the simulations at 300 and 350 K were already well equilibrated in the 400 K simulations so that it took less time to re-equilibrate them at the lower temperatures. This allows us to run the shorter simulations at 300 and 350 K. It should be noted that a similar time interval of ~300 ps in the equilibrated regions of the trajectories was used at all temperatures to calculate the Li diffusivity in the smaller system.

The temperature fluctuations were within the 100 K interval, with an rms deviation of ~50 K. The integration time step was 1 fs. The cell parameters are $a = b = 10.080$ and $c = 14.200$ Å for 83Li/2[TFSI], and $a = b = 11.554$ and $c = 22.442$ Å for 164Li/4[TFSI] at 400 K.

The ionic diffusion coefficient D was derived from the corresponding MSD curve using the Einstein diffusion equation, which could be written as follows:

$$\mathrm{MSD}(t) \equiv \left\langle (r(t) - r(t_o))^2 \right\rangle = 6\mathrm{D}t$$

and E_a from the Arrhenius equation for diffusion,

$$\mathrm{D}(T) = \mathrm{D}_o \exp(-E_a/RT).$$

Published under license by AIP Publishing

In addition to the conventional MSD method, we used the 2PT methodology[32–35] to calculate the diffusion coefficients. The 2PT methodology obtains accurate entropy and free energy information from short (~20 ps) dynamics, allowing for analysis during reactions and phase transitions. The 2PT approach uses the velocity autocorrelation function

$$C(t) = \sum_{j=1}^{N}\sum_{k=1}^{3} mj\left[\lim_{t\to\infty}\frac{1}{2\tau}\int_{-\tau}^{\tau} v_j^k(t'+t)v_j^k(t')dt'\right]$$

and takes the Fourier transform to obtain the vibrational density of states, DoS(υ),

$$\mathrm{DoS}(\nu) = \frac{2}{kT}\sum_{j=1}^{N}\sum_{k=1}^{3} m_j s_j^k(\nu) = \frac{2}{kT}\lim_{t\to\infty}\int_{-\tau}^{\tau} C(t)e^{-i2\pi\nu t}dt,$$

which is corrected for diffusional contributions and then used to calculate entropy, free energy, and other thermodynamic properties by applying quantum statistics. Moreover, this can be done atom by atom to understand the variations in the local entropy and free energy across the interfaces. The density of states at zero frequency is related to the diffusion constant (D): $\mathrm{DoS}(0) = 12mD/kT$, where m – mass of atoms, N – number of atoms, D – diffusivity of atoms, k – the Boltzmann constant, and T – temperature. Indeed, the component of DoS(0) on each atom gives an accurate measure of the diffusion constant for that atom.

See the supplementary material for MSD for Li atoms in the Li-metal region and SEI CL, and temperature dependences of the Li-diffusion coefficient based on the MSD and 2PT results.

This work was supported by a research grant from LG Chem. S.M. is thankful for the support by Act 211 Government of the Russian Federation, under Grant No. 02.A03.21.0011 and by the Supercomputer Simulation Laboratory of the South Ural State University.[63]

REFERENCES

[1]G. B. Appetecchi, G. T. Kim, M. Montanina, M. Carewska, R. Marcilla, D. Mecerreyes, and I. De Meatza, "Ternary polymer electrolytes containing pyrrolidinium-based polymeric ionic liquids for lithium batteries," J. Power Sources **195**, 3668–3675 (2010).

[2]S. F. Lux, M. Schmuck, S. Jeong, S. Passerini, M. Winter, and A. Balducci, "Li-ion anodes in air-stable and hydrophobic ionic liquid-based electrolyte for safer and greener batteries," Int. J. Energy Res. **34**, 97–106 (2010).

[3]G. T. Kim, S. S. Jeong, M. Z. Xue, A. Balducci, M. Winter, S. Passerini, F. Alessandrini, and G. B. Appetecchi, "Development of ionic liquid-based lithium battery prototypes," J. Power Sources **199**, 239–246 (2012).

[4]L. E. Barrosse-Antle, A. M. Bond, R. G. Compton, A. M. O'Mahony, E. I. Rogers, and D. S. Silvester, "Voltammetry in room temperature ionic liquids: Comparisons and contrasts with conventional electrochemical solvents," Chem.—Asian J. **5**, 202–230 (2010).

[5]H. Kim, Y. Ding, and P. A. Kohl, "LiSICON—Ionic liquid electrolyte for lithium ion battery," J. Power Sources **198**, 281–286 (2012).

[6]G. B. Appetecchi, M. Montanino, and S. Passerini, "Ionic liquid-based electrolytes for high-energy lithium batteries in ionic liquids science and applications," in *ACS Symposium Series 1117*, edited by A. E. Visser, N. J. Bridges, and R. D. Rogers (Oxford University Press, Inc., American Chemical Society, Washington, DC, USA, 2013).

[7]P. Guan, L. Liu, and X. Lin, "Simulation and experiment on solid electrolyte interphase (SEI) morphology evolution and lithium-ion diffusion," J. Electrochem. Soc. **162**, A1798–A1808 (2015).

[8]A. Wang, S. Kadam, H. Li, S. Shi, and Y. Qi, "Review on modeling of the anode solid electrolyte interphase (SEI) for lithium-ion batteries," npj Comput. Mater. **4**, 15 (2018).

[9]X.-B. Cheng, R. Zhang, C.-Z. Zhao, F. Wei, J. G. Zhang, and Q. Zhang, "A review of solid electrolyte interphases on lithium metal anode," Adv. Sci. **3**, 1500213 (2016).

[10]E. Peled and S. J. Menkin, "Review—SEI: Past, present and future," J. Electrochem. Soc. **164**, A1703–A1719 (2017).

[11]S. Xiong, K. Xie, E. Blomberg, P. Jacobsson, and A. Matic, "Analysis of the solid electrolyte interphase formed with an ionic liquid electrolyte for lithium-sulfur batteries," J. Power Sources **252**, 150–155 (2014).

[12]L. Liu, J. Park, X. Lin, A. M. Sastry, and W. Lu, "A thermal-electrochemical model that gives spatial-dependent growth of solid electrolyte interphase in a Li-ion battery," J. Power Sources **268**, 482–490 (2014).

[13]M. Brousselya, S. Herreyreb, P. Biensan, P. Kasztejnac, K. Nechevc, and R. J. Staniewic, "Aging mechanism in Li ion cells and calendar life predictions," J. Power Sources **97-98**, 13–21 (2001).

[14]N. Takenaka, Y. Suzuki, H. Sakai, and M. Nagaoka, "On electrolyte-dependent formation of solid electrolyte interphase film in lithium-ion batteries: Strong sensitivity to small structural difference of electrolyte molecules," J. Phys. Chem. C **118**, 10874–10882 (2014).

[15]B. V. Merinov, S. V. Zybin, S. Naserifar, S. Morozov, J. Oppenheim, W. A. Goddard III, J. Lee, J. H. Lee, H. E. Han, Y. C. Choi, and S. H. Kim, "Interface structure in Li-metal/[Pyr_{14}][TFSI]-ionic liquid system from *ab initio* molecular dynamics simulations," J. Phys. Chem. Lett. **10**, 4577–4586 (2019).

[16]F. Shi, P. Pei, D. T. Boyle, J. Xie, X. Yu, X. Zhang, and Y. Cui, "Lithium metal stripping beneath the solid electrolyte interphase," Proc. Natl. Acad. Sci. U. S. A. **115**, 8529–8534 (2018).

[17]D. D. Macdonald, "The point defect model for the passive state," J. Electrochem. Soc. **139**, 3434–3449 (1992).

[18]P. C. Howlett, N. Brack, A. F. Hollenkamp, M. Forsyth, and D. R. MacFarlaned, "Characterization of the lithium surface in N-methyl-N-alkylpyrrolidinium bis(trifluoromethanesulfonyl)amide room-temperature ionic liquid electrolytes," J. Electrochem. Soc. **153**, A595–A606 (2006).

[19]J. Yan, B. J. Xia, Y. C. Su, X. Z. Zhou, J. Zhang, and X. G. Zhang, "Phenomenologically modeling the formation and evolution of the solid electrolyte interface on the graphite electrode for lithium-ion batteries," Electrochim. Acta **53**, 7069–7078 (2008).

[20]L. Benitez and J. M. Seminarioa, "Ion diffusivity through the solid electrolyte interphase in lithium-ion batteries," J. Electrochem. Soc. **164**, E3159–E3170 (2017).

[21]P. Verma, P. Maire, and P. Novak, "A review of the features and analyses of the solid electrolyte interphase in Li-ion batteries," Electrochim. Acta **55**, 6332–6341 (2010).

[22]M. Nie, D. Chalasani, D. P. Abraham, Y. Chen, A. Bose, and B. L. Lucht, "Role of solution structure in solid electrolyte interphase formation on graphite with $LiPF_6$ in propylene carbonate," J. Phys. Chem. C **117**, 25381–25389 (2013).

[23]P. P. R. M. L. Harks, F. M. Mulder, and P. H. L. Notten, "*In situ* methods for Li-ion battery research: A review of recent developments," J. Power Sources **288**, 92–105 (2015).

[24]A. M. Andersson and K. Edström, "Chemical composition and morphology of the elevated temperature SEI on graphite," J. Electrochem. Soc. **148**, A1100–A1109 (2001).

[25]F. Kong, R. Kostecki, G. Nadeau, X. Song, K. Zaghib, K. Kinoshita, and F. McLarnon, "*In situ* studies of SEI formation," J. Power Sources **97-98**, 58–66 (2001).

[26]A. M. Andersson, D. P. Abraham, R. Haasch, S. MacLaren, J. Liu, and K. Amine, "Surface characterization of electrodes from high power lithium-ion batteries," J. Electrochem. Soc. **149**, A1358–A1369 (2002).

[27]X. H. Liu and J. Y. Huang, "*In situ* TEM electrochemistry of anode materials in lithium ion batteries," Energy Environ. Sci. **4**, 3844–3860 (2011).

[28]P. Lu and S. J. Harris, "Lithium transport within the solid electrolyte interphase," Electrochem. Commun. **13**, 1035–1037 (2011).

[29]I. V. Veryovkin, C. E. Tripa, A. V. Zinovev, S. V. Baryshev, Y. Li, and D. P. Abraham, "TOF SIMS characterization of SEI layer on battery electrodes," Nucl. Instrum. Methods Phys. Res., Sect. B **332**, 368–372 (2014).

Published under license by AIP Publishing

[30]D. Bar-Tow, E. Peled, and L. Burstein, "A study of highly oriented pyrolytic graphite as a model for the graphite anode in Li-ion batteries," J. Electrochem. Soc. **146**, 824–832 (1999).
[31]A. M. Andersson, A. Henningson, H. Siegbahn, U. Jansson, and K. Edström, "Electrochemically lithiated graphite characterised by photoelectron spectroscopy," J. Power Sources **119-121**, 522–527 (2003).
[32]S.-T. Lin, P. K. Maiti, and W. A. Goddard III, "Two-phase thermodynamic model for efficient and accurate absolute entropy of water from molecular dynamics simulations," J. Phys. Chem. B **114**, 8191–8198 (2010).
[33]T. A. Pascal, S.-T. Lin, and W. A. Goddard III, "Thermodynamics of liquids: Standard molar entropies and heat capacities of common solvents from 2PT molecular dynamics," Phys. Chem. Chem. Phys. **13**, 169–181 (2011).
[34]T. A. Pascal, W. A. Goddard, and T. Jung, "Entropy and the driving force for the filling of carbon nanotubes with water," Proc. Natl. Acad. Sci. U. S. A. **108**, 11794–11798 (2011).
[35]T. A. Pascal, Y. He, S. Jiang, and W. A. Goddard III, "Thermodynamics of water stabilization of carboxybetaine hydrogels from molecular dynamics simulations," J. Phys. Chem. Lett. **2**, 1757–1760 (2011).
[36]T. A. Pascal, W. A. Goddard, P. K. Maiti, and N. Vaidehi, "Role of specific cations and water entropy on the stability of branched DNA motif structures," J. Phys. Chem. B **116**, 12159–12167 (2012).
[37]J. Pan, "General method to predict voltage-dependent ionic conduction in a solid electrolyte coating on electrodes," Phys. Rev. B **91**, 134116 (2015).
[38]S. Jurng, Z. L. Brown, J. Kima, and B. L. Lucht, "Effect of electrolyte on the nanostructure of the solid electrolyte interphase (SEI) and performance of lithium metal anodes," Energy Environ. Sci. **11**, 2600–2608 (2018).
[39]D. Strmcnik, I. E. Castelli, J. G. Connell, D. Haering, M. Zorkol, P. Martins, P. P. Lopes, B. Genorio, T. Østergaard, H. A. Gasteiger, F. Maglia, B. K. Antonopoulos, V. R. Stamenkovic, J. Rossmeisl, and N. M. Markovic, "Electrocatalytic transformation of HF impurity to H_2 and LiF in lithium-ion batteries," Nat. Catal. **1**, 255–262 (2018).
[40]R.-S. Kühnel and A. Balducci, "Lithium ion transport and solvation in N-butyl-N-methylpyrrolidinium bis(trifluoromethanesulfonyl)imide–Propylene carbonate mixtures," J. Phys. Chem. C **118**, 5742–5748 (2014).
[41]K. Oldiges, D. Diddens, M. Ebrahiminia, J. B. Hooper, I. Cekic-Laskovic, A. Heuer, D. Bedrov, M. Winterabd, and G. Brunklaus, "Understanding transport mechanisms in ionic liquid/carbonate solvent electrolyte blends," Phys. Chem. Chem. Phys. **20**, 16579–16591 (2018).
[42]F. Castiglione, E. Ragg, A. Mele, G. B. Appetecchi, M. Montanino, and S. Passerini, "Molecular environment and enhanced diffusivity of Li^+ ions in lithium-salt-doped ionic liquid electrolytes," J. Phys. Chem. Lett. **2**, 153–157 (2011).
[43]G. A. Elia, U. Ulissi, S. Jeong, S. Passerini, and J. Hassoun, "Exceptional long-life performance of lithium-ion batteries using ionic liquid-based electrolytes," Energy Environ. Sci. **9**, 3210–3220 (2016).
[44]L. L. Daemen, J. F. Browning, M. Doucet, N. J. Dudney, and G. M. Veith, "Lithium transport in an amorphous Li_xSi anode investigated by quasi-elastic neutron scattering," J. Phys. Chem. C **121**, 11083–11088 (2017).
[45]H.-H. Chiang, J.-M. Lu, and C.-L. Kuo, "First-principles study of the structural and dynamic properties of the liquid and amorphous Li-Si alloys," J. Chem. Phys. **144**, 034502 (2016).
[46]H.-J. Deiseroth, S.-T. Kong, H. Eckert, J. Vannahme, C. Reiner, Y. Zaiβ, and M. Schlosser, "Li_6PS_5X: A class of crystalline Li-rich solids with an unusually high Li^+ mobility," Angew. Chem., Int. Ed. **47**, 755–758 (2008).
[47]R. P. Rao and S. Adams, "Studies of lithium argyrodite solid electrolytes for all-solid-state batteries," Phys. Status Solidi A **8**, 1804–1807 (2011).
[48]N. J. J. de Klerk, I. Roslon, and M. Wagemaker, "Diffusion mechanism of Li argyrodite solid electrolytes for Li-ion batteries and prediction of optimized halogen doping: The effect of Li vacancies, halogens, and halogen disorder," Chem. Mater. **28**, 7955–7963 (2016).
[49]J. Auvergniot, A. Cassel, J.-B. Ledeuil, V. Viallet, V. Seznec, and R. Dedryvère, "Interface stability of argyrodite Li_6PS_5Cl toward $LiCoO_2$, $LiNi_{1/3}Co_{1/3}Mn_{1/3}O_2$, and $LiMn_2O_4$ in bulk all-solid-state batteries," Chem. Mater. **29**, 3883–3890 (2017).
[50]T. Cheng, B. V. Merinov, S. Morozov, and W. A. Goddard, "Quantum mechanics reactive dynamics study of solid Li-electrode/Li_6PS_5Cl-electrolyte interface," ACS Energy Lett. **2**, 1454–1459 (2017).
[51]S. Wenzel, S. J. Sedlmaier, C. Dietrich, W. G. Zeier, and J. Janek, "Interfacial reactivity and interphase growth of argyrodite solid electrolytes at lithium metal electrodes," Solid State Ionics **318**, 102–112 (2018).
[52]G. Kresse and J. Furthmuller, "Efficiency of *ab-initio* total energy calculations for metals and semiconductors using a plane-wave basis set," Comput. Mater. Sci. **6**, 15–50 (1996).
[53]G. Kresse and J. Furthmuller, "Efficient iterative schemes for *ab initio* total-energy calculations using a plane-wave basis set," Phys. Rev. B **54**, 11169–11186 (1996).
[54]G. Kresse and D. Joubert, "From ultrasoft pseudopotentials to the projector augmented-wave method," Phys. Rev. B **59**, 1758–1775 (1999).
[55]J. Perdew, K. Burke, and M. Ernzerhof, "Generalized gradient approximation made simple," Phys. Rev. Lett. **77**, 3865–3868 (1996).
[56]S. Grimme, J. Antony, S. Ehrlich, and H. Krieg, "A consistent and accurate *ab initio* parametrization of density functional dispersion correction (DFT-D) for the 94 elements H-Pu," Chem. Phys. **132**, 154104 (2010).
[57]S. Grimme, S. Ehrlich, and L. Goerigk, "Effect of the damping function in dispersion corrected density functional theory," J. Comput. Chem. **32**, 1456 (2011).
[58]M. Aykol, S. Kim, and C. W. van der Waals, "Interactions in layered lithium cobalt oxides," J. Phys. Chem. C **119**(33), 19053–19058 (2015).
[59]K. V. Kravchyk, P. Bhauriyal, L. Piveteau, C. P. Guntlin, B. Pathak, and M. V. Kovalenko, "High-energy-density dual-ion battery for stationary storage of electricity using concentrated potassium fluorosulfonylimide," Nat. Commun. **9**, 4469 (2018).
[60]A. Kabiraj and S. Mahapatra, "High-throughput first-principles-calculations based estimation of lithium ion storage in monolayer rhenium disulfide," Commun. Chem. **1**, 81 (2018).
[61]H. Yildirim, J. B. Haskins, C. W. Bauschlicher, Jr., and J. W. Lawson, "Decomposition of ionic liquids at lithium interfaces. 1. *Ab initio* molecular dynamics simulations," J. Phys. Chem. C **121**, 28214–28234 (2017).
[62]J. B. Haskins, H. Yildirim, C. W. Bauschlicher, Jr., and J. W. Lawson, "Decomposition of ionic liquids at lithium interfaces. 1. Gas phase computations," J. Phys. Chem. C **121**, 28235–28248 (2017).
[63]P. Kostenetskiy and P. Semenikhina, "SUSU supercomputer resources for industry and fundamental science," in Proceedings of 2018 Global Smart Industry Conference, GloSIC, 2018, 8570068.

Published under license by AIP Publishing